LIGHT DRIVEN REDUCTION OF CARBON DIOXIDE VIA RUTHENIUM POLYPYRIDYL COMPLEXES IN THE PRESENCE OF A PYRIDINIUM COCATALYST

by

MATTHEW WEST

Presented to the Faculty of the Graduate School of

The University of Texas at Arlington in Partial Fulfillment

of the Requirements

for the Degree of

MASTER OF SCIENCE IN CHEMISTRY

THE UNIVERSITY OF TEXAS AT ARLINGTON

May 2015

Acknowledgements

Science to me is about the journey as well as the results so in turn there are those I would like to acknowledge. First and foremost are all of the coworkers that I have closely worked with since I started my graduate career. There has always been a feeling of teamwork throughout along with help when you need a second opinion.

There are many teachers and faculty members that I would like to thank such as Dr. Jimmy Rogers for encouraging me throughout my undergraduate days. Dr. William Cleaver and Dr. Heide Conrad have been an inspiration in educating others in what I have studied along with helping me to understand different approaches to problems. I would like to thank Dr. David Boston who helped forward my understanding of chemistry before and after he moved on to brighter things. I would never have accomplished my goals without the support of my friends and family thus I would like to thank my parents Jerry and Sue Ann West and everyone else who stood by me during my academic career.

What most do not know about me is that my love of chemistry started in high school where my teacher showed us some amazing things and since then I was hooked. That being said I would like to thank and acknowledge my former high school chemistry teacher Mr. Bruce McHam who is studying for his medical degree at UT Southwestern.

Dr. Purnendu Dasgupta graciously opened his lab in order to run ion chromatography for which I can't thank Brian Stamos enough with his help in obtaining those results.

My final acknowledgement goes out to the man who has guided me through my graduate career. He has helped me understand chemistry on new levels and pushed me to research on my own. I thank Dr. Frederick MacDonnell for all of his encouragement over the two years that I have worked in his lab. Sometimes in the face of how little you

actually know and understand it is hard to move forward and try you must. In Dr. MacDonnell's words "That's why they put the RE in re-search".

April 16, 2015

Abstract

LIGHT DRIVEN REDUCTION OF CARBON DIOXIDE VIA RUTHENIUM POLYPYRIDYL COMPLEXES IN THE PRESENCE OF A PYRIDIUM CATALYST

Matthew West, M.S.

The University of Texas at Arlington, 2015

Supervising Professor: Frederick MacDonnell

The rapid increase in atmospheric carbon dioxide since the industrial revolution is now beginning to cause global climate changes which could adversely affect our planets ecosystem. Nonetheless, our ability to sustain the current world population and standard of living relies on cheap and abundant energy which is only currently obtainable from the continued use of fossil fuels, which further add CO_2 to the atmosphere. Given these circumstances, there is considerable interest and urgency in the development of new technology which would help us replace fossil fuels with fuels derived from sustainable energy sources, and in particular, the sun. In particular, a process for the solar-driven reduction of CO_2 into useful liquid transportation fuels, such as methanol, could lead to a carbon-neutral fuel cycle and eliminate the need for fossil fuels. If photochemical processes are to be developed along these lines, the incident solar radiation, which is predominantly in the visible portion of the electromagnetic spectrum, must be effectively absorbed by photocatalysts which then go on to drive the desired reactions.

Ru(II) and Re(II) transition metal complexes are among the most widely studied chromophores for solar fuel photochemical processes. In particular, $[Ru(phen)_3]^{2+}$

$Ru(bpy)_3]^{2+}$, $[Ru(tpy)_2]^{2+}$, and more recently $[Ru(bqp)_2]^{2+}$ (where bpy = 2,2'-bipyridine, tpy = 2,2':6',2''-terpyridine, and bqp = 2,6-di(quinolin-8-yl)pyridyl) have enjoyed considerable attention due to their good chemical stability and promising photophysical properties, including good absorption in the visible and long lived ^{3}MLCT states. In this thesis, these complexes were studied computationally to determine what factors affect their excited state lifetimes, which are seen to vary from 0.25 ns to 3 □s. Previous researchers have proposed an electronic model in which thermal population of triplet metal centered states from the ^{3}MLCT state is the key factor in determining excited state lifetime. The closer in energy that the two excited states are, the faster is the non-radiative decay. In this study, we examine the structural features including ligand structure, denticity, metal-ligand bond angles, and deviations from octahedral geometry and correlate these factors to the excited state lifetime, in view of the existing electronic model. The calculations show that the HOMO is metal centered (t_{2g} in O_h) whereas the LUMO is ligand centered (□*) The LUMO+1 has mixed ligand □* and metal e_g character, the extent of which depends strongly on the degree of distortion from O_h symmetry, as measured by the bond angles about the metal center. The greater the degree of distortion, the greater the e_g character of the LUMO+1 and also the closer in energy it is to the LUMO. Thermal population of energetically similar excited states [(t_{2g}^5 – □*^{1} (LUMO)] and [t_{2g}^5 – (□*+e_g)^1 (LUMO+1)] provides an alternative non-radiative pathway for vibrationally returning to the ground state via population of a state that has appreciable metal d-d character. Overall, this electronic description of the molecule provides an accurate mechanistic understanding of the dominant non-radiative decay pathway.

In chapter 2, we report on the use of $[Ru(bpy)_3]^{2+}$ and $[Ru(bqp)_2]^{2+}$ as chromophores for the photocatalytic reduction of CO_2 to methanol using pyridinium co-catalysts. Bocarsly and coworkers have shown that a mixture of pyridine and pyridinium

in water (pH 5.5) is an effective electrocatalytic system for CO_2 reduction to methanol. In 2013 MacDonnell and coworkers, reported that the pyridine/pyridinium CO_2 reduction chemistry could be driven photochemically using $[Ru(phen)_3]^{2+}$ as a co-catalsyt. In this chapter, this photochemical activity is examined with the related $[Ru(bpy)_3]^{2+}$, and the $[Ru(bqp)_2]^{2+}$ chromophores, which are expected to show improved activity due to improved cage escape yields and longer excited state lifetimes, respectively. The bipyridine system produced 83±6 μM (0.4 TON) of methanol which was an increase of 20 μM from the control while it produced a very small amount of formate until roughly 4 hours had elapsed. It is possible for formate to enter the catalytic cycle and be reduced to methanol. The photocatalytic system using $[Ru(bqp)_2]^{2+}$ as a chromophore produced 40 μM (0.7 TON) of methanol with a reduced starting concentration.

Table of Contents

List of Illustrations

List of Tables

List of Schemes

Chapter 1

Computational Analysis of Ruthenium Polypyridyl Catalysts

1.1 Introduction

Scientists around the world have become increasingly concerned while continuing to watch rising levels of carbon dioxide in the Earth's atmosphere. If levels of carbon dioxide continue to rise, it is predicted to have devastating effects for our planets ecosystem due to drastic changes in the Earth's climate. Studies conducted by, Willner Meyer, Bocarsly, and others have been done over the years involving the use of transition metal complexes and catalysts to work in helping the environment by reducing carbon dioxide via solar and electrical power.[1, 2, 3]

Photocatalysis is the process where light is absorbed by a chromophore to generate an excited state electron-hole pair, which is then used to drive an endergonic redox processes and regenerate the photocatalyst. Transition metal complexes, and in particular ruthenium polypyridyl complexes, are excellent chromophores for photoredox reactions as they are strong absorbers in the visible region and have favorable photophysical properties.[4, 5] In particular the energetics of the various excited-state and ground-state complexes accessible by these chromophores bridge the energy gap needed to split water into H_2 and O_2. The species accessible for $[Ru(bpy)_3]^{2+}$ and their reduction potentials are shown below in a modified Latamier-type diagram, where $[Ru(bpy)_3]^{2+*}$ indicated the photoexcited molecule.

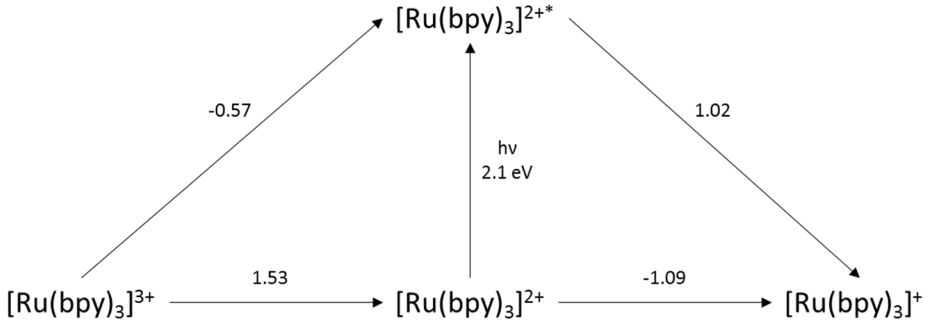

Figure 1-1: Latimer-diagram of $[Ru(bpy)_3]^{2+}$ by Meyer in its ground and photoexcited states with redox potentials vs NHE.

A localized view of photocatalytic process starts with the excitation of an electron in the t_{2g} orbitals centered on the ruthenium (II) ion to the empty pyridine ligand π^* orbitals, commonly known as a metal-to-ligand charge transfer (MLCT) excitation.[6, 7] If the hole in the t_{2g} orbital left by the excited electron is rapidly filled by electron-transfer from a sacrificial electron donor (also known as reductive quenching of the excited state), such as ascorbate, the electron in the ligand □* orbital becomes trapped there and is a potent one-electron reductant (e.g. $[Ru(bpy)_3]^+$).[8] While written as $[Ru(bpy)_3]^+$ the complex is best described as a Ru(II) ion, two bpy, and one bpy radical anion, and thus the reduced complex has a reduction potential comparable to an aromatic radical anion (less the losses due to electrostatics). With a reduction potential of 1.02 V vs NHE, such a species is more than adequate to drive the reduction of protons to H_2, or CO_2 to CO or methanol. The absorption in the visible, that occurs at 480 nm (2.5 eV), is assigned as the MLCT process previously mentioned. The initial product is a ^{1}MLCT state but studies have shown fast and quantitative intersystem crossing to a ^{3}MLCT state, which can be stable for nanoseconds to microseconds.[6] The excited state can decay by two 'non-reactive' pathways: i. it can emit a photon (luminescence, radiative decay) or ii. it can vibrationally relax (non-radiative decay) to the ground state, as shown in Figure 1-2, where k_r and k_{nr} indicate the rate constants for radiative and non-radiative decay respectively. The lifetime of the excited state is generally dominated by non-radiative decay as radiative decay is usually a slow process.[9, 10] Because these chromophores are conformationally rigid, vibrational

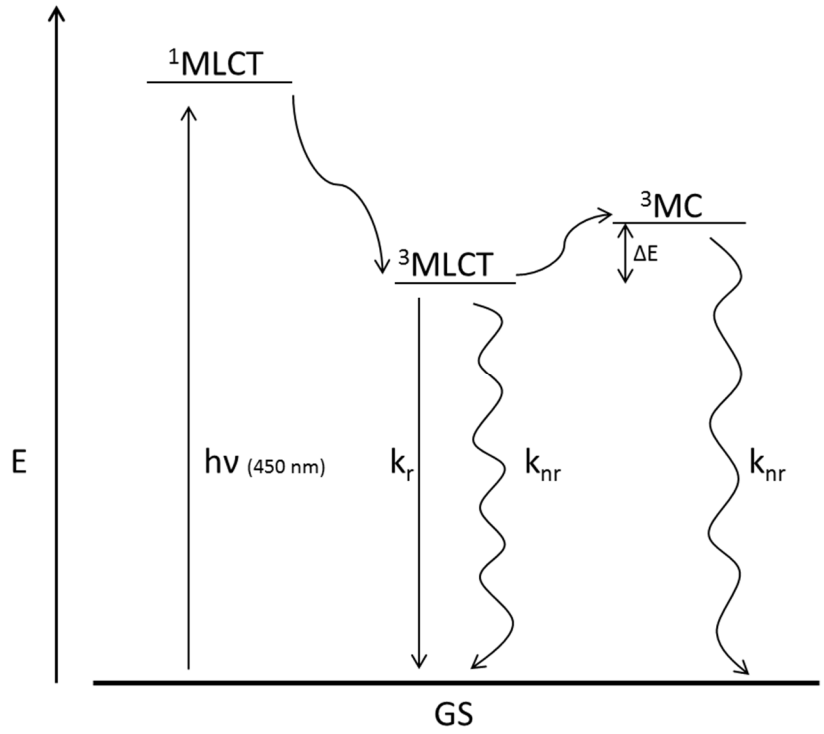

Figure 1-2: Jablonski diagram of photoexcitation.

deactivation is slow and the photoexcited state can participate in redox reactions with donors or acceptors, thereby transferring some of the excited state potential to chemical potential. The longer-lived the photoexcited state, the greater its chances are of participating in an electron-transfer reaction with a donor or acceptor.[6, 11] The excited state half-life, denoted as τ, which is propotional to k_r/k_{nr}. Thus an understanding of the dominant factors for k_{nr} is essential if we are to be able to design and prepare chromophores with long-lived excited states. The predominant model for non-radiative decay is that thermal promotion of the photoexcited electron from a ^{3}MLCT state into a low-lying metal-centered (^{3}MC) state (which is formally □* in character) is responsible for most of the deactivation.[6, 12] This model puts the e_g acceptor orbital above the ligand □* MO, as shown in Figure 1-3, and predicts that if the energy gap between these two MOs in increased, thermal population of the associated ^{3}MC state will be lessened and the excited-state lifetime will increase.

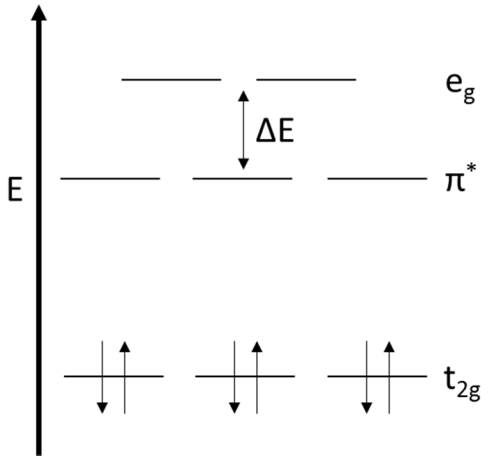

Figure 1-3: Octahedral Molecular Orbital Diagram with ligand centered orbitals.

Recently, a computational study by Persson et. al. concluded that lifetime is not dependent on Δ_o,[6] or the change in energy of the metal *d* orbitals, which conflicts with this model. Table 1-1 contains some structure and photophysical data for four related ruthenium polypyridyl complexes: ruthenium(II) tris(1,10-phenanthroline), ruthenium(II) tris(2,2-bipyridine), ruthenium(II) bis(terpyridine), and ruthenium(II) di(2,6-bis(quinolin-8-yl)pyridyl). As can be seen, the excited state lifetimes can vary considerably even though all of these complexes have the same basic d^6 low-spin electronic structure. Prior to Persson's study it was theorized that the short lifetime of $[Ru(tpy)_2]^{2+}$ was due to the closeness of the ^{3}MLCT state to a triplet metal-centered (^{3}MC) state.[12] As the tpy ligand has some bite angle restraints due to formation of two adjacent 5 membered rings, it distorts the metal center from pure octahedral which would have a trans N-Ru-N bond angle, known as Θ and depicted in Figure 1-4, of 180 deg to 156.6 deg![13] The ligand bite angle is depicted as Φ.

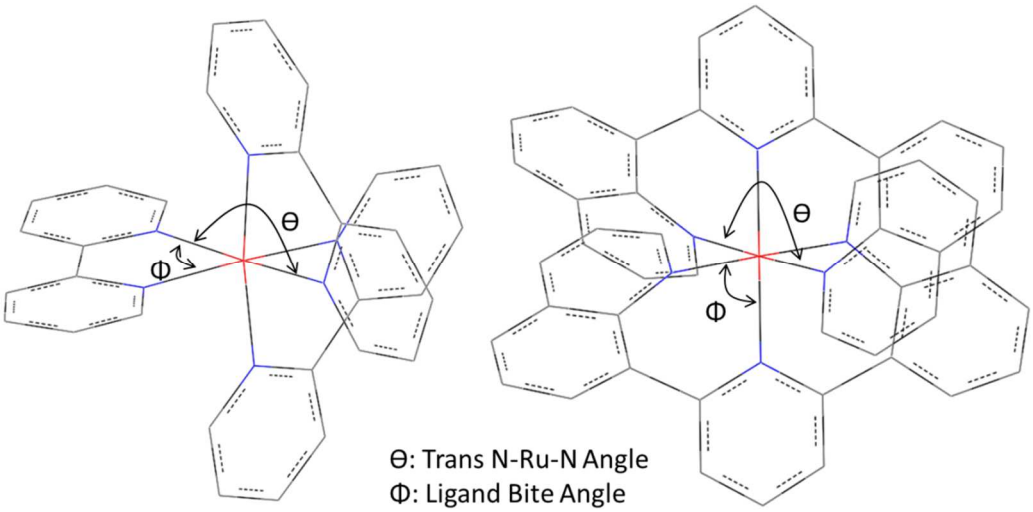

Figure1-4: Crystal structures denoting angles on bidentate (left) and tridentate (right) complexes.

The distortion was thought to lower the Δ_o for the complex, bringing the e_g MO closer to the ligand π^*. This explanation seemed reasonable given that the bpy and phen complexes, which show a lower degree of O_h distortion, and the bqp complex, with almost ideal O_h symmetry, exhibit lifetimes that increase as the distortion is lowered.[14] In this case the distortion is measured as the trans N-Ru-N angle either on the tridentate ligand or the trans N-Ru-N for a meridonal arrangement of two nitrogens from one bidentate ligand an one nitrogen from another bidentate ligand. Both are depicted in Figure 1-4.

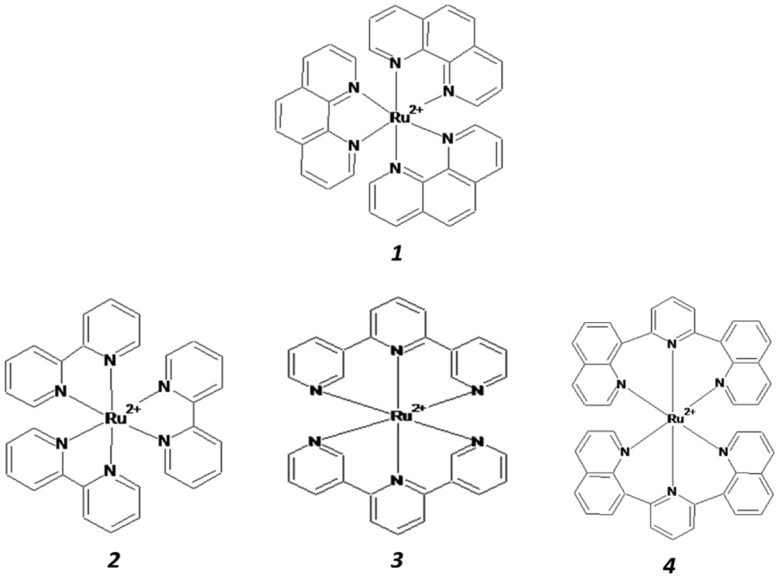

Figure 1-5: Chemical structures of $[Ru(phen)_3]^{2+}$ (1), $[Ru(bpy)_3]^{2+}$ (2), $[Ru(tpy)_2]^{2+}$ (3), and $[Ru(bqp)_2]^{2+}$ (4).

Table 1-1: Table showing denticity, trans N-Ru-N angle, lifetime emissions, absorbance, and molar extinction coefficient for all complexes.

Complex	Denticity	Θ	τ_{ns}	Calc. Abs (nm)	Exp. Abs (nm)	Extinction Coefficient (M-1cm-1)
$[Ru(tpy)_2]^{2+}$	k^2	156.6°	0.25[15]	415	476[11]	10,000[11]
$[Ru(phen)_3]^{2+}$	k^3	173.1°	~800	396	453	19,000[16]
$[Ru(bpy)_3]^{2+}$	k^3	173.0°	~1000[15]	432	453	18,000
$[Ru(bqp)_2]^{2+}$	k^2	178.5°	3000[14]	467	485	14,000[14]

Recently reported by MacDonnell and Boston was a photocatalytic system that included $[Ru(phen)_3]^{2+}$ as a chromophore. There have been intensive computational studies performed by Zheng for both $[Ru(phen)_3]^{2+}$ and $[Ru(bpy)_3]^{2+}$, but a comparison between tridentate $[Ru(tpy)_2]^{2+}$ and $[Ru(bqp)_2]^{2+}$ with the existing chromophore $[Ru(phen)_3]^{2+}$ has not been done.[7, 17, 6] In this study, we examined the molecular orbital structures of $[Ru(bpy)_3]^{2+}$, $[Ru(tpy)_2]^{2+}$, and $[Ru(bqp)_2]^{2+}$ using the Becke three-parameter Lee Yang Parr computational method. Our goal was to compare the molecular orbitals of these complexes to an existing photocatalytic complex in the

hopes that they would prove to be a more proficient chromophore. After optimization of the calculated structures, we compared these data with available X-ray structural data and previously reported computations shown in Table 1-2. The degree of distortion was measured as a function of the trans N-Ru-N angles (Θ) as described above and associated with their emission lifetimes. An analysis of the orbital contributions, particularly for the LUMO and LUMO+1 was then used to correlate orbital composition with the observed lifetime data. Orbital energies were compared to determine if any dependence emerged with excited-state emission lifetimes. The next section will take viable chromophores and judge their effectiveness in a photocatalytic system in comparison to the already reported $[Ru(phen)_3]^{2+}$ system.[11]

1.2 Experimental

1.2.1 Geometry Optimization and Frequency Computations

All structures were optimized with the same set of commands and the same procedures. The method was a ground state density functional theory (DFT) Becke three-parameter Lee Yang Parr (B3LYP) calculation, using Gaussian09, which is highly utilized for these complexes in todays' literature.[18, 19, 7, 17] The cc-pVDZ basis set was used for all non-metals where a LanL2DZ basis set was used specifically for the ruthenium. All complexes were in a +2 charged state and optimized in an unrestricted conductor polarizable continuum model (CPCM) to model the charged species in solution using an aqueous solvent model to match the experimental parameters. All optimizations were performed with tight self consistent field (SCF) convergence criteria to produce more accurate results along and ultra-fine integral grids, as recommended in the Gaussian documentation in order to accurately compute large molecules.[17] For brevity, the optimization and frequency computations were done at the same time. Orbital pictures are shown in subsequent sections.

1.2.2 Absorbance Computations

Absorbance spectrums were generated for all complexes in order to determine absorbance and effect of E_g and T_{2g} splitting due to symmetry changes. The computations were formed using Time-Dependent DFT with the same basis sets and solvent model as the optimizations for computing the first twenty excited states. A comparison of calculated absorbance values along with actual experimental comparisons will be seen later on.

1.3 Computational Results and Discussion

1.3.1 Optimization of Ruthenium(II) tris(1,10-phenanthroline)

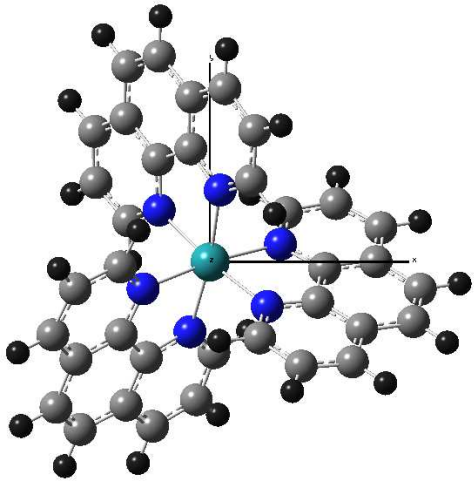

Figure 1-6: Optimized structure of $[Ru(phen)_3]^{2+}$

Figure 1-6 above shows the optimized structure of $[Ru(phen)_3]^{2+}$. The structure is tris-bidentate with a bite angle of 78.7°, and a N-Ru-N angle of 173° suggesting a distorted octahedral structure. Reported experimental bite angle and trans N-Ru-N, seen in table 1-2, was 79.8° and 173.1 respectively.[20] Previous computations were also referenced for the ligand bite angle of 79.4°.[7] The difference of the calculated angles can be attributed to slight difference of basis sets that were used for the literature optimizations but the computations differ from experimental data by 1.1°. Shown below in Figure 1-7 are orbital images of the HOMO, LUMO, and LUMO+1 of the complex which show the calculated electron densities around the ligand and

metal for these complexes. The HOMO is centered on the *d*- orbitals of the metal with small ligand interaction. The LUMO is composed of the ligand *p*-orbitals. The LUMO+1 orbital contains both *d* and *p* character with Zheng calculating the orbital to have 6.4% *d*-character.[7] Since the HOMO and LUMO orbitals contribute to spectral properties an MLCT transfer would take place upon excitation.

As stated previously, the non-radiative decay of the electron back to the ground state was undesirable. The smaller *d*-character present in the ligand orbitals stabilizes the excited ^{1}MLCT state that the electron occupies (LUMO+1) as reported in literature. It has already been used in a successful photocatalytic system, thus $[Ru(phen)_3]^{2+}$ can be compared to the other complexes as a reference or control. Knowing that this complex is an active chromophore we can assume that its ^{3}MLCT state is different than its ^{3}MC state where intersystem crossing is unfavored.

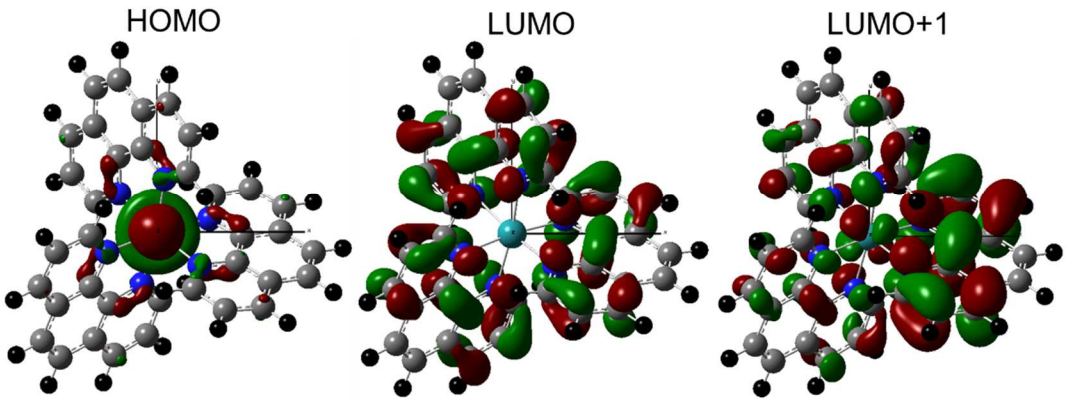

Figure 1-7: Electron density images of $[Ru(phen)_3]^{2+}$. The energies are -6.15 eV, -2.52 eV, and -2.43 eV respectively.

1.3.2 Optimization of Ruthenium(II) tris(2,2'-bipyridine)

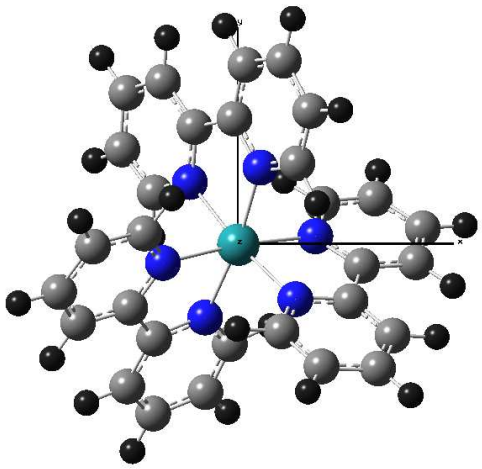

Figure 1-8: Optimized structure of $[Ru(bpy)_3]^{2+}$

The ruthenium(II) tris(bipyridine) structure shown above in Figure 1-8 is highly similar to that of $[Ru(phen)_3]^{2+}$. Its structure is also tris-bidentate. The calculated bite angle (Φ) and trans N-Ru-N angle (Θ) were 77.7° and 172.9° respectively. These angles were slightly different than calculated and experimental by Zheng who calculated the bite angle to be 78.4° and 78.7° respectively.[17] The experimental trans N-Ru-N from known crystal structures was found to be 173°.[21] This matches the calculated angle almost exactly. Cause of the difference in the calculated bite angle could be from the lack of a solvent system used in previous computations. Electron density orbital images are shown below for this complex.

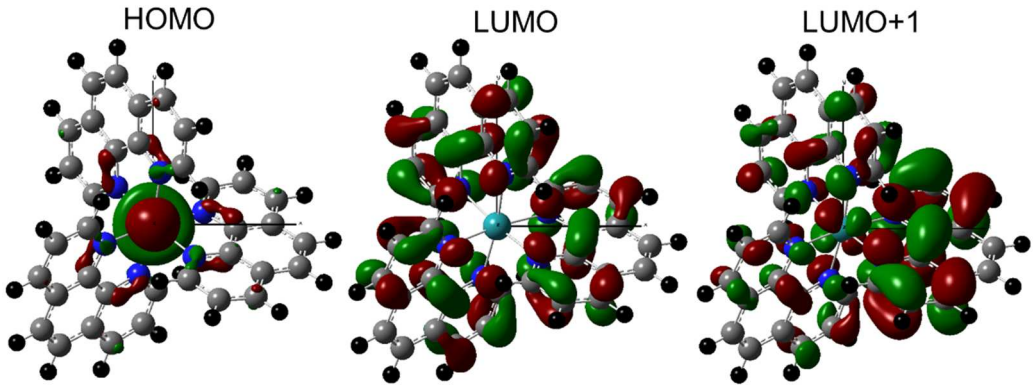

Figure 1-9: Electron density images of $[Ru(bpy)_3]^{2+}$. The energies are from left to right -6.19 eV, -2.64 eV, and -2.54 eV respectively.

From these images that were generated in Figure 1-9 we can see the main HOMO and potentially all HOMO orbitals have metal-centered *d*-character while the LUMO orbitals are centered with *p*-character of the ligands, specifically the carbon atoms. Some LUMO orbitals such as the LUMO+1 have a small amount of *d* character contributing where it is previously reported by Zheng to be 6.2%, which is also slightly smaller than the previous ruthenium(II) tris(1,10-phenanthroline) control.[17, 7] Zheng also computed that the LUMO of $[Ru(bpy)_3]^{2+}$ included more ligand character than $[Ru(phen)_3]^{2+}$. This type of electron density suggests an ^{3}MLCT type of excitation similar to the control, $[Ru(phen)_3]^{2+}$. The LUMO+1's slightly less *d*-character stabilizes the electron in the ligand orbitals.

1.3.3 Optimization of Ruthenium(II) bis(2,2':6',2''-terpyridine)

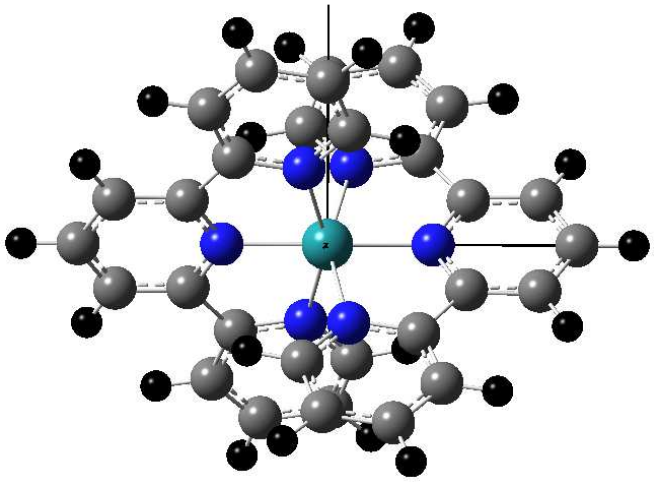

Figure 1-10: Optimized structure of $[Ru(tpy)_2]^{2+}$

From the previous complexes we know that emission lifetime is increases with greater ligand involvement and lower metal *d* electron involvement. This stabilizes the electron on the ligands and thus extends the emission lifetime of the excited state. Moving to tridentate structure seemed the most logical step to limit octahedral distortion and increase emission lifetime. The bipyridine structure had a longer emission lifetime than the control so from there a terpyridine structure was looked at. The bite and trans N-Ru-N angles of the terpyridine complex were calculated to be 78.3° and 156.6° respectively. The bite angle was similar to the angle of the control of $[Ru(phen)_3]^{2+}$ (78.7°), but the N-Ru-N angle was reduced to 156.6° creating a significant octahedral distortion. Persson calculated angles of 78.4° and 184.6° while Hammarström and Lashgari experimentally concluded it to be 79.5° and 159.1° from its crystal structure.[12, 13, 12] All angles are compared in Table 1-2. Below in Figure1-10 shows how this distortion affects the orbital densities for $[Ru(tpy)_2]^{2+}$.

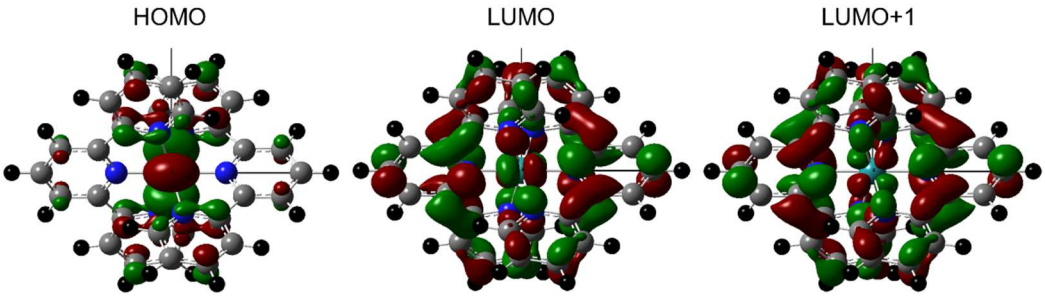

Figure 1-11: Electron Density images of $[Ru(tpy)_2]^{2+}$. The energies are -6.29 eV, -2.7 eV, and -2.7 eV.

Compared to $[Ru(phen)_3]^{2+}$ and $[Ru(bpy)_3]^{2+}$, the terpyridine complex has significantly more metal *d*-orbital character in its LUMO and LUMO+1 orbital. Calculated to be over 7%. This mixing allows the electron to relax to the ground state on the metal very quickly by aligning its ^{3}MLCT state with an ^{3}MC state that it can be obtained through intersystem crossing. The short life time makes this complex unsuitable as a photocatalyst.

1.3.4 Optimization of Ruthenium(II) bis(2,6-Di(quinolin-8-yl)pyridyl)

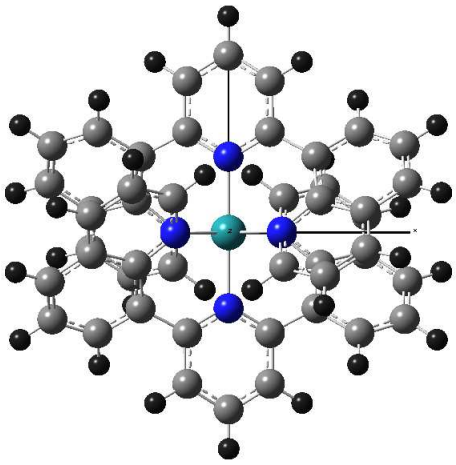
Figure 1-12: Optimized structure of $[Ru(bqp)_2]^{2+}$

The structure of $[Ru(bqp)_2]^{2+}$ shown in Figure 1-12 was computed using the same outlines previously stated. The structure matches the reported literature.[22] Similar to the previous complex, $[Ru(bqp)_2]^{2+}$ is also tridentate though it has vastly different angles, 89.3° and 178.5° compared to $[Ru(tpy)_2]^{2+}$ (78.3° and 156.6°). The angles slightly differ with a previous study

conducted by Hammarström where the angles were experimentally determined from the crystal structure to be 89.8° and 177.6°.[14] Both bite and trans N-Ru-N angles signify that the complex has more octahedral symmetry, is less distorted, than any of the previous complexes studied earlier. With an emission lifetime over three times that of $[Ru(phen)_3]^{2+}$, we confirm symmetry or rather Δ_o does not affect the lifetime of the ^{3}MLCT excited-state but rather that of the ^{3}MC state.[6] Persson et. Al. has shown that the LUMO and LUMO+1 of $[Ru(bqp)_2]^{2+}$ have little to no *d*-character from the E_g orbitals. With little to no *d*-character the ^{3}MC state is vastly different than the ^{3}MLCT state and therefore an intersystem crossing is unlikely to occur. Other studies conducted by Persson using near perfect octahedrals such as ruthenium(II) di(2,6-bis(2-pyridylmethyl)pyridine) proved not to have an improvement on lifetime. It was theorized that conformationally nonrigid structure was to blame as rotation around the methyls allowed for more excited state distorton.[6]

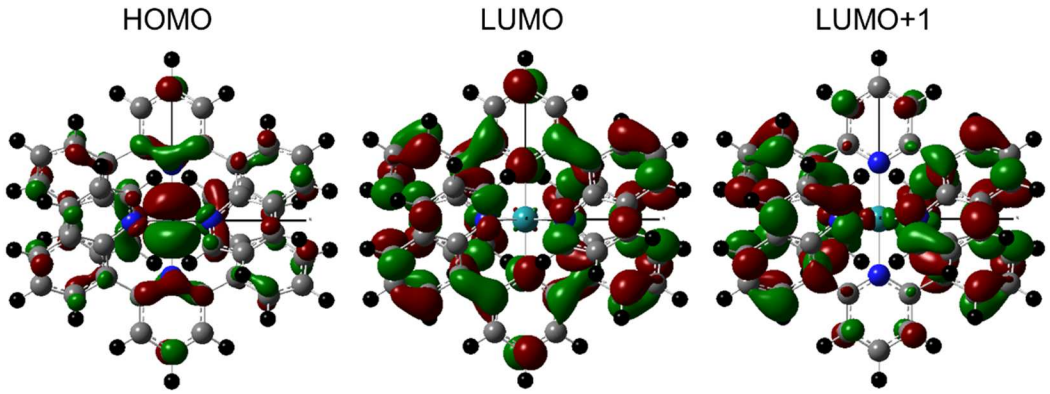

Figure 1-13: Electron density images of $[Ru(bqp)_2]^{2+}$. The energies are -5.92eV, -2.75eV, and -2.64eV.

In Figure 1-13 above we see a slight difference in the electron densities between $[Ru(bqp)_2]^{2+}$ and the ones that came before it. This complex has minute *d*-character (1%) in the LUMO orbitals than the previous complexes as well as more *p* character in its HOMO orbital but compared to previous complexes the *d*-character of the LUMO+1 orbital is drastically smaller

giving it the ability to stabilize its ^{1}MLCT state and ^{3}MLCT state and not allowing for much intersystem crossing to an undesired ^{3}MC state which only relaxes vibrationally.[12] These energies and figures closely match known literature. All angles are given in Table 1-2 with their respective references.

Table 1-2: Comparison of calculated and experimental ligand bite angles (Φ) and trans N-Ru-N angles (Θ).

Complex	Φ (degrees)			Θ (degrees)		
	Calc.	Calc$_{ref}$	Exp$_{ref}$	Calc.	Calc$_{ref}$	Exp$_{ref}$
$[Ru(tpy)_2]^{2+}$	78.3	78.4[6]	78.6[23]	156.6	184.6[6]	159.1[13]
$[Ru(phen)_3]^{2+}$	78.7	79.4[7]	79.8[20]	173		173.1[20]
$[Ru(bpy)_3]^{2+}$	77.7	78.4[17]	78.7[17]	172.9		173[21]
$[Ru(bqp)_2]^{2+}$	89.3	89.8[14]	88.9[14]	178.5	179[6]	177.6[14]

1.3.5 Molecular Orbital HOMO – LUMO Gap Comparison

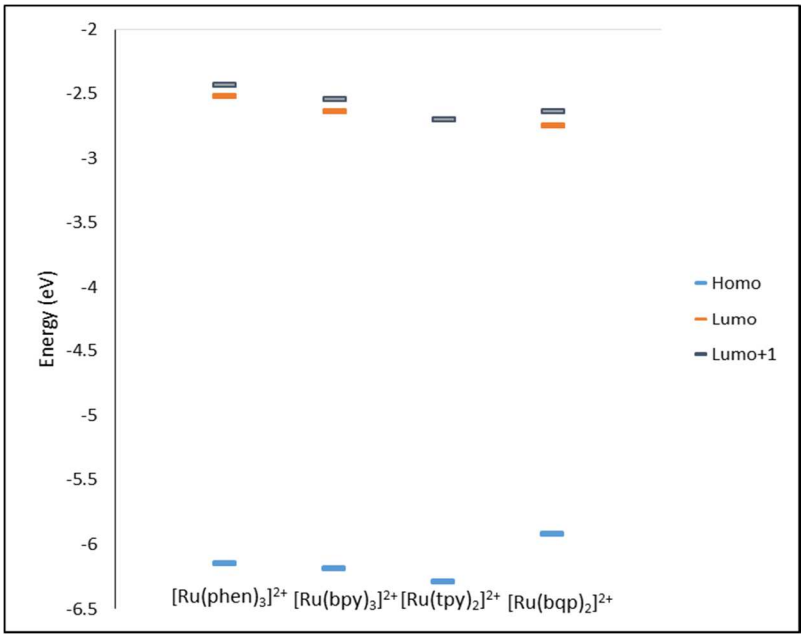

Figure 1-14: Molecular orbital comparison of complexes.

Figure 1-14, is a comparison of the molecular orbital energies of all complexes observed. The figure shows a decreasing energy difference in the HOMO and LUMO states. The shrinking of the HOMO-LUMO energy gap indicates the complexes have better octahedral symmetry around the metal. This means that less energy is needed to effect an electronic transition. The use of less energy to effect an electronic transition should show what is called a "red shift" in the absorbance spectra which is shown next.[10, 12] Figure 1-14 also displays a crucial difference in the LUMO and LUMO+1 orbitals. $[Ru(tpy)_2]^{2+}$ which is known to have a very small excited-state lifetime (0.25 ns) has virtually no separation, or a very minute amount, between the LUMO and LUMO+1 orbitals meaning very small to no difference between its triplet and singlet MLCT states. This, and taking into account the electron density for its π*, we can assume that upon excitation the electron populates directly into a state that is metal-centered. If we assume that the orbitals are degenerate with one another the metal character is then doubled (14%). The largest separation of LUMO and LUMO+1 is in $[Ru(bqp)_2]^{2+}$ where the largest excited-state lifetime has been recorded.

1.3.6 UV-Vis computations and Experimentation

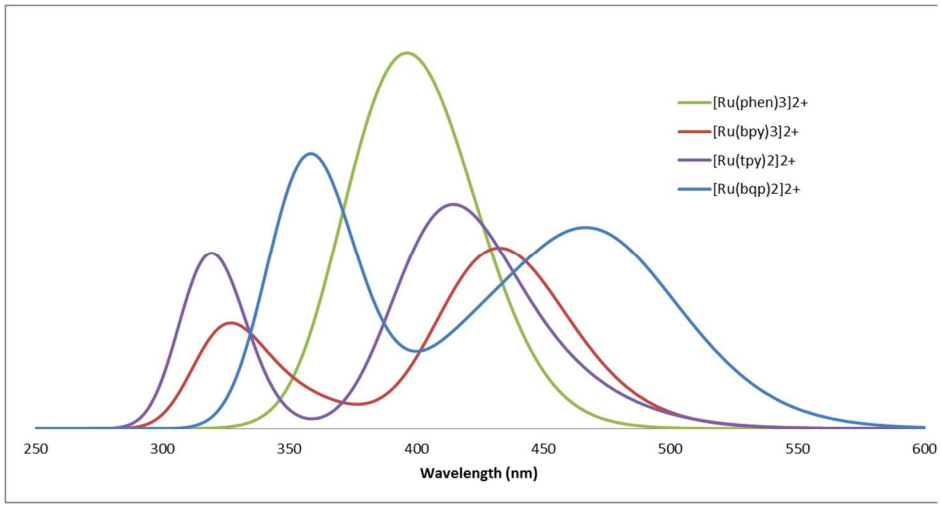

Figure 1-15: Absorbance of Complexes. $[Ru(phen)_3]^{2+}$ (396 nm); $[Ru(bpy)_3]^{2+}$ (432 nm); $[Ru(tpy)_2]^{2+}$ (415 nm); $[Ru(bqp)_2]^{2+}$ (467 nm)

Figure 1-15 is evidence of a shrinking HOMO-LUMO gap which was then confirmed by Absorbance both calculated and experimental which are Figures 1-15 and 1-16 respectively. Absorbance computations were done using a Time-Dependent function. A shrinking of this gap means that there should be a corresponding shift towards higher wavelengths or ("red shift") which is shown in Figure 1-15. This data conflicts with literature in the epsilon values that were obtained as well as differing solvent systems causing absorbance maxima to be altered, yet the trend remains the same.[24, 25, 18, 11] Experimental data confirms the shift in Figure 1-16 below except for $[Ru(tpy)_2]^{2+}$ as this complex is unfit to be used as a photocatalyst and thus was not tested experimentally. Figure 1-16 shows the experimental absorbance of complexes $[Ru(phen)_3]^{2+}$, $[Ru(bpy)_3]^{2+}$, and $[Ru(bqp)_2]^{2+}$. $[Ru(bqp)_2]^{2+}$ has a red shifted MLCT absorbance band at approximately 490 nm. While both $Ru(phen)_3]^{2+}$ and $[Ru(bpy)_3]^{2+}$ absorb at approximately 454 nm.

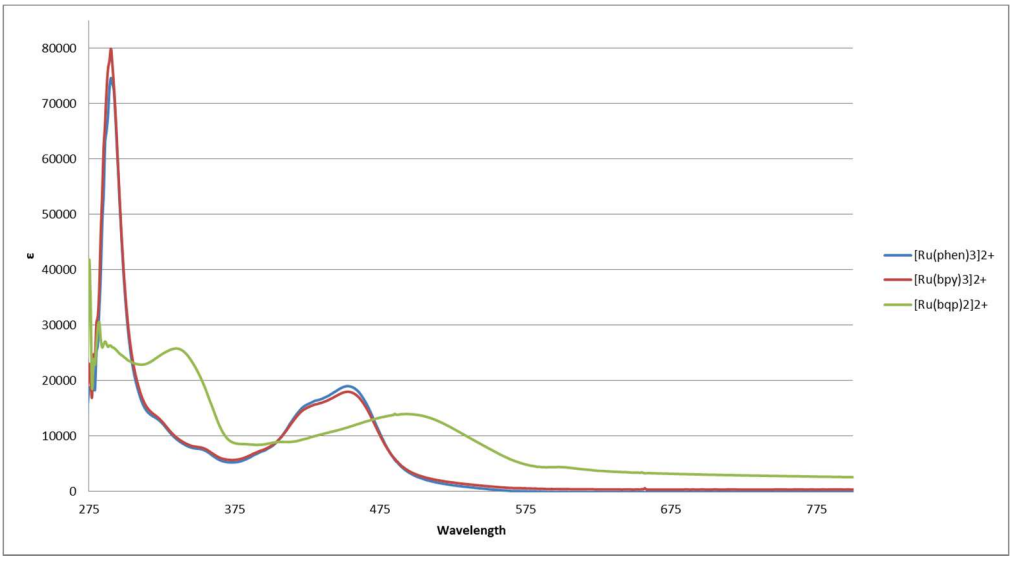

Figure 1-16: Absorbance data for $[Ru(phen)_3]^{2+}$(blue), $[Ru(bpy)_3]^{2+}$(red), and $[Ru(bqp)_2]^{2+}$(green) using a 1cm cuvette and unknown concentrations.

1.4 Conclusion

These computations can only point a direction to go. It is clear that the best photocatalyst is $[Ru(bqp)_2]^{2+}$, due to its small *d*-character in the LUMO and LUMO+1 orbitals which helps to stabilize the MLCT states and destabilize its ^{3}MC states, while the worst would be $[Ru(tpy)_2]^{2+}$ for the opposite reason.[12] $[Ru(bpy)_3]^{2+}$ should not be counted out as it has a better emission lifetime and less *d*-character in its MLCT states than the control. Like a previous study by Persson, there was no evidence to suggest denticity or Δ_o have any relation to the excited state emission lifetime although, from the complexes tested the emission lifetime did have a direct dependence on the trans N-Ru-N angle (Θ) to the ruthenium metal center shown in Figure 1-17.[6]

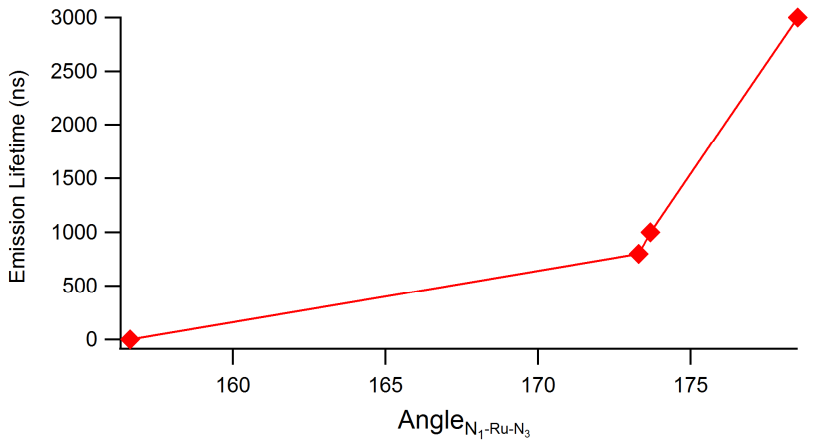

Figure 1-17: Emission lifetime dependence of the ^{3}MLCT excited state vs. ligand Trans N-Ru-N (θ) angle for all complexes.

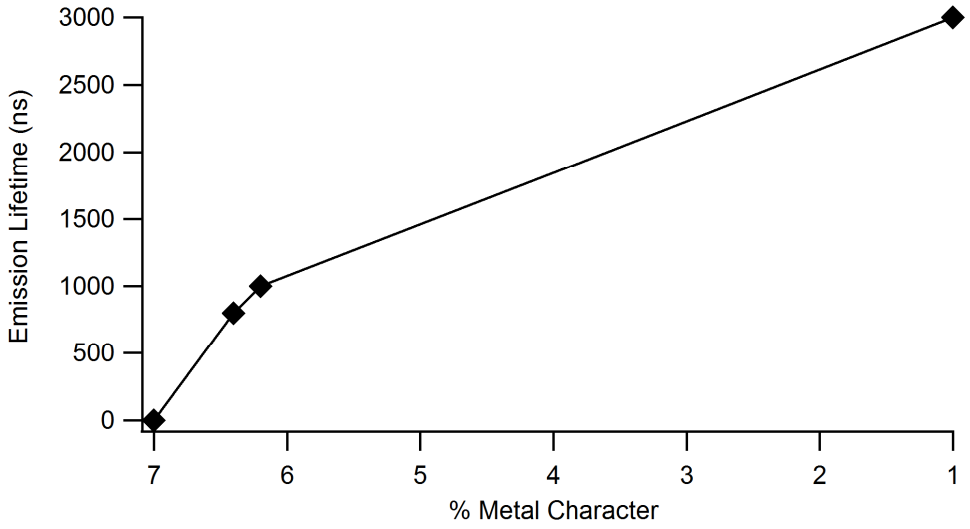

Figure 1-18: Graph depicting excited-state emission lifetime vs percent metal character of complexes.

Emission lifetime did increase with decreasing distortion. Distortion from octahedral allows greater mixing between the e_g and π* orbitals. This mixing promotes intersystem crossing from the ^{3}MLCT state to a ^{3}MC state where the electron can vibrationally relax faster to the metal without emitting a photon.[6] This is supported by Figure 1-18 where it is depicted that lifetime emission decreases with increasing percent metal character of the LUMO+1 orbital. Degeneracy of the terpyridine complex was not taken into account in this figure.

Chapter 2

Photocatalytic Reduction of Carbon Dioxide under Constant Pressure

2.1 Introduction

In the past decade, the world's focus has shifted towards the environment amid concerns of global warming. In physics, it is called cause and effect, with the cause being the industrial revolution and the effect being rising levels of carbon dioxide in our atmosphere from the burning of fossil fuels. As carbon dioxide builds in our atmosphere, global climate changes are predicted to occur and worsen over time. From this concern, research into the conversion of carbon dioxide back into usable fuels has increased dramatically as it is hoped that a sustainable, carbon-neutral fuel cycle can be developed. Methanol is the simplest carbon-based fuel molecule that is a liquid and represents a particularly valuable fuel as it can be easily integrated into today's fuel infrastructure.[4] If light or solar energy could be used to effectively drive the reduction of CO_2 to methanol, then it is possible that an environmentally friendly fuel cycle could be developed.[4] Scheme 2-2 shows a balanced redox reaction for the reduction of carbon dioxide to methanol using ascorbate as the electron/proton donor. In an ideal situation this donor would be water, which would be oxidized to O_2.

Carbon dioxide is the most stable and oxidized form of carbon. From Figure 2-1, which is shown below, the first reduction of carbon dioxide to its radical species has the largest reduction potential.[5] It is this activation barrier that makes reducing carbon dioxide challenging thus requiring a catalyst. A number of different homogeneous catalysts have been developed to reduce carbon dioxide but most can't reduce CO_2 to useable products such as methanol, six electron reduction, and methane which is an eight electron reduction.[2, 26]

$CO_2 + e^- \rightarrow CO_2^{\bullet-}$ $E^\circ = -1.90$ V

$CO_2 + 2\ e^- + 2\ H^+ \rightarrow CO + H_2O$ $E^\circ = -0.53$ V

$CO_2 + 2\ e^- + 2\ H^+ \rightarrow HCOOH$ $E^\circ = -0.61$ V

$CO_2 + 4\ e^- + 4\ H^+ \rightarrow H_2CO + H_2O$ $E^\circ = -0.48$ V

$CO_2 + 6\ e^- + 6\ H^+ \rightarrow H_3COH + H_2O$ $E^\circ = -0.38$ V

$CO_2 + 8\ e^- + 8\ H^+ \rightarrow CH_4$ $E^\circ = -0.24$ V

Figure 2-1: Reductions of carbon dioxide with their respective potentials.[5]

Bocarsly and coworkers showed that carbon dioxide could be electrocatalytically reduced using pyridine and/or pyridinium as the electrocatalyst.[27] The mechanism by which pyridine does this is complicated by the fact that the electrode material is important for the electrocatalysis and thus seems to play an active role in the process. This has led to several competing theoretical studies regarding the actual role of the surface and overall mechanism..[28, 29, 30] A simple surface-free mechanism involves the formation of pyridinium radicals and subsequent carbamate adducts as illustrated in Scheme 2-1.

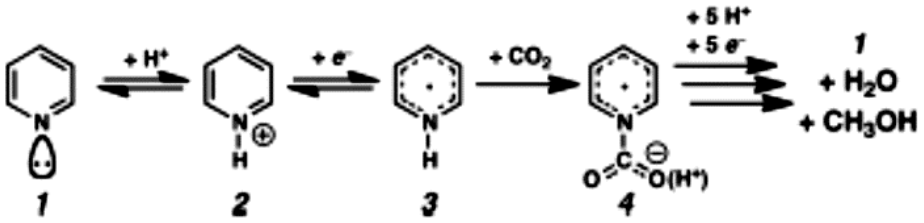

Scheme 2-1: One postulated mechanism for the six-electron reduction of carbon dioxide to methanol catalyzed by pyridinium.

Bocarsly's system required Pt, Pd or p-GaP electrodes where the reduction potential of the pyridinium radical shifts to a more positive nature.[31, 32] This shift is not seen when using glassy carbon or Hg electrodes along with significantly less methanol production. From here homogeneous pyridine-based reduction of carbon dioxide is theorized to be unsuccessful or plagued with issues. Seeking to solve this issue MacDonnell et al successfully produced the first

homogeneous pyridine-based system capable of reducing carbon dioxide to methanol by using $[Ru(phen)_3]^{2+}$ as a photosensitive chromophore and ascorbate as a sacrificial donor.[4] Scheme 2-2 shows a balanced redox reaction for the reduction of carbon dioxide to methanol using an ascorbate as the electron/proton donor. In an ideal situation this donor would be water, which would be oxidized to O_2.

Bocarsly's success with the use of pyridinium ion to selectively electrocatalytically reduce CO_2 to methanol suggested that a photochemical process for this transformation may be viable. MacDonnell and Boston reported that $[Ru(phen)_3]^{2+}$ and pyridine in water (pH 5.0) worked synergistically to photocatalytically reduce CO_2 to methanol and formate. In this case, water was not the donor. Instead potassium ascorbate was used as a donor, as reductive quenching of the photoexcited state of $[Ru(phen)_3]^{2+}$ and $[Ru(phen)_3]^{2+}$ with this donor was already known to be fast and irreversible.[33, 34] In order to use water as the terminal donor, a competent water oxidation co-catalyst needs to be developed that also reacts quickly with the excited state ruthenium complex. To date, no such co-catalyst exists although it is the subject of considerable research.[35]

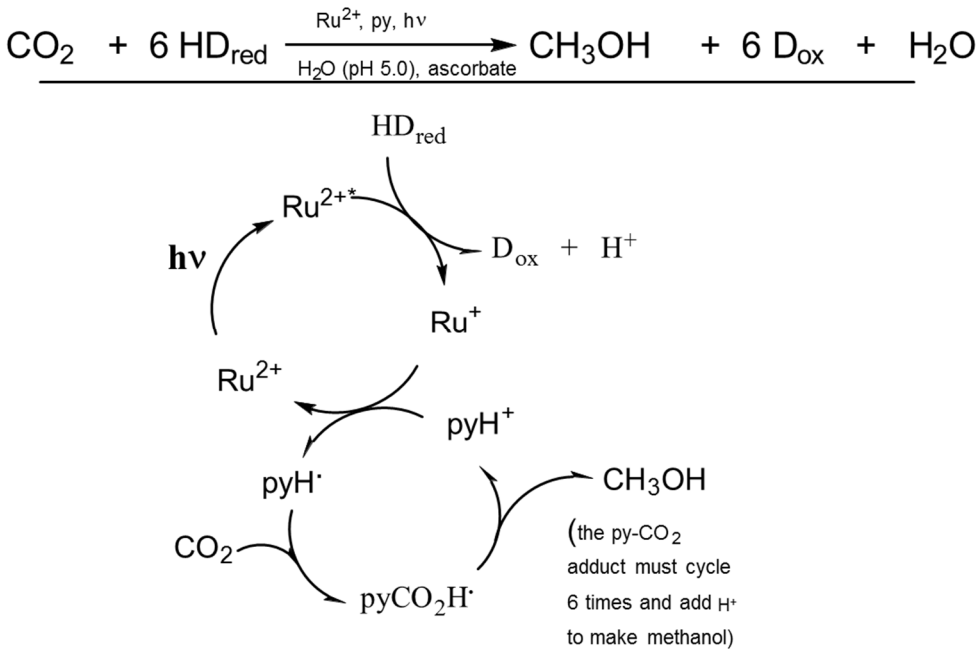

Scheme 2-2: The net chemical reaction for the photochemical reduction of CO_2 with ascorbate (top), and the putative catalytic cycles occurring during the process (bottom).

The net chemical reaction and putative catalytic cycle are shown in Scheme 2-2, where Ru^{2+} signifies a typical Ru(II) polypyridyl chromophore. In the above scheme, MacDonnell also reported that potassium chloride (KCl) but not LiCl, NaCl, RbCl, or CsCl or alkaline earth salts, increased methanol production.[4] The reason for this was not well understood but it has been proposed that this cation may have the appropriate size to ion-pair and stablize some of the carbamate intermediates proposed in the cycle. Subsequently, MacDonnell and Boston also showed that chromophore and pyridine co-catalyst could be combined in a single unimolecular photocatalyst, however this system was inactive in pure water and required mixed-solvents (i.e. 1 M H_2O in DMF) for good activity.[36] This unimolecular photocatalyst was more selective towards methanol generation over formate than the bimolecular system and of comparable activity. Nonetheless, the presence of DMF greatly complicated the product detection and mixed solvent systems are far less desirable than aqueous solution, so further efforts were invested in the

aqueous system. It was proposed that moving to a tridentate ligand structure may help increase the effectiveness of the chromophore. As discussed in the previous chapter the distortion from octahedral seems to encourage mixing between the e_g and π^* orbitals thus destabilizing the MLCT states of the complex. Moving to a tridentate complex could then provide a conformationally rigid structure where octahedral distortions could be severally diminished.

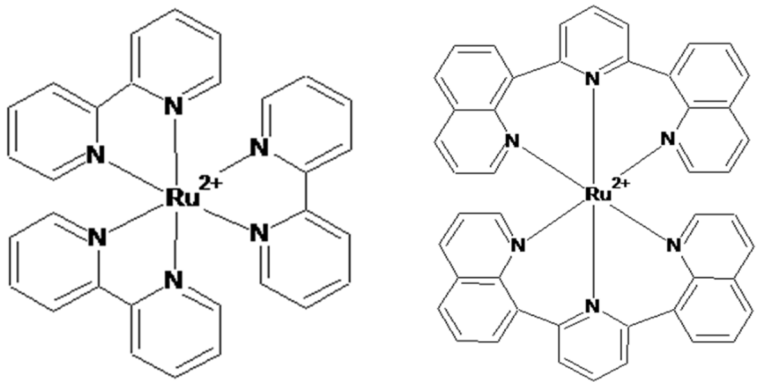

Figure 2-2: Chemical structure of $[Ru(bpy)_3]^{2+}$ (left), and $[Ru(bqp)_2]^{2+}$ (right).

This thesis reports on the behavior of two other ruthenium(II) polypyridyl chromophores in the bimolecular photocatalytic system. $[Ru(bpy)_3]^{2+}$ and $[Ru(bqp)_2]^{2+}$, shown in Figure 2-2, are promising chromophores with surprisingly different photochemical and sometimes photophysical behavior than $[Ru(phen)_3]^{2+}$. $[Ru(bpy)_3]^{2+}$ In particular, Castellano and co-workers reported that the cage escape yields for $[Ru(phen)_3]^{2+}$ and $[Ru(bpy)_3]^{2+}$ with ascorbate were surprisingly different, at <10% and 55%, respectively.[35, 37, 38] The cage escape yield is a measure of the fraction of solvent caged $[[Ru(L\text{-}L)_3]^{+}\cdots Asc_{ox}]$ pairs that dissociate prior to electron transfer back to the ascorbate radical. As seen, $[Ru(bpy)_3]^{2+}$ is 25 times more effective in generating the key reduced $[Ru(bpy)_3]^{+}$ complex, however it should be noted that as a trischelate complex it is subject to the same type of ligand dissociation reactions that are responsible for deactivating the $[Ru(phen)_3]^{2+}$ chromophores. The $[Ru(bqp)_2]^{2+}$ chromophore has the stability advantages of the $[Ru(tpy)_2]^{2+}$ complex with a long-lived excited state lifetime at room temperature in fluid solution.[6]

Thus we proposed that a study of the bipyridine and 2,6-di(quinolin-8-yl)pyridyl chromophores may well surpass the performance of the $[Ru(phen)_3]^{2+}$ chromophore in terms of stability and quantum yield.

2.2 Experimental

2.2.1 Photolysis

All metal complexes were prepared as described in the literature.[22, 39, 24] Commercial reagent grade ascorbic acid has been recrystallized from methanol and contains trace quantities of methanol that skew the experimental results. The following procedure was used to remove these trace impurities. Ascorbic acid (10 g) was dissolved in 20 mL millipore water and filtered if necessary. The water was then removed by rotary evaporation using a warm (55 °C) water bath. This procedure was repeated a total of six times. Pyridine was distilled before use. All water was obtained from a Millipore purification system.

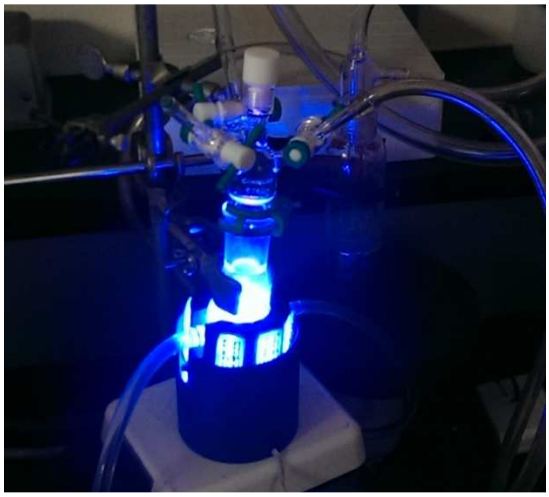

Figure 2-3: Photoreactor used in all photolysis experiments.

The photoreactor, shown above in Figure 2-3, that was used for all photolysis reactions used 120 LED lights (5 mm dim) connected in parallel circuits of 24 that produced light at 470 nm ±20 nm. All glassware was blown out of borosilicate glass with > 90% transmittance in 330 nm-

1000 nm range. The reaction vessel is a two part system with the outer space serving as a borosilicate water jacket with inlet and outlet adapters.[4] The inner reaction space can contain a stir bar and holds approximately 30 mL of solution. The top consists of a custom adapter designed with three 2 mm stopcocks at 120° around a threaded 7 mm top opening designed for a UV-Vis adapter. All pieces fit snuggly together with grease to make sure pressure is held. Rubber bands were used to maintain a tight seal from the adapter to the reaction vessel. Carbon dioxide was bubbled into the 25 mL solution for 30 minutes. In a typical experiment, the photoreactor was charged with 0.2 M ascorbic acid, 0.1 M potassium chloride, 0.05 M pyridine, 49 μM acetonitrile as an internal standard, and 225 μM of the chromophore. A sample was taken as t=0 and the lamp was then turned on. Samples were then collected at 30 min, 1 h, 4 h, 6 h, and 8 h. Samples (2 mL) were taken through septa to hold pressure inside the reactor and placed in 10 mL headspace vials.

2.2.2 Product Analysis

Headspace analysis was performed using a Zebron ZB-BAC2 blood alcohol gas chromatograph column which measured 30 m in length, 0.32 mm in diameter, and had a film thickness of 1.2 μm. The separation method was an isotherm for the first 2 minutes followed by a 20°/min increase until 45° at which it was held at constant temp for the duration of the run (7.25 min). Total run time was 10 minutes. The Shimadzu Gas Chromatograph 2010Plus was paired with a Shimadzu TQ8040 Mass Spectrometer in Selected Ion Monitoring (SIM) mode.[40] Analysis was done with carrier gas consisting of helium (120 kPa) and argon (40 kPa). The mass detector was specifically targeting 29 m/z (formaldehyde), 31 m/z (methanol), 41 m/z (acetonitrile), and 45 m/z (formic acid). Methanol and acetonitrile were the only peaks that were able to be quantified. All analysis used a Shimadzu AOC-5000Plus headspace autosampler which agitated and heated the samples at 80°C for 30 minutes prior to injection (500 μL) with an 80°C headspace needle. A sample chromatogram is shown in Figure 2-6.

Ion chromatography was performed with the assistance of Mr. Brian Stamos using an AG24 guard column with an AS24 separatory column. Each sample was prepared using a Dionex Onguard II Ag/H ion filter using the manufacturer's recommended procedures. Samples were kept at 20°C while being run at a 30°C isotherm on an IC1000 chromatograph. A sample chromatogram is shown in Figure 2-8.

2.3 Results and Discussion

2.3.1 Methanol Production with Carbon Dioxide

2.3.1.1 System using $[Ru(phen)_3]^{2+}$

MacDonnell and Boston previously showed that photocatalytic reduction of CO_2 and using $[Ru(phen)_3]^{2+}$ and pyridine, yielded methanol and formate. This system produced 66 μM of methanol after 6 hours and 18 mM of formate after the first hour. It was determined that the major product of the reaction was formate.[4] A significant difference in our system is the constant pressure seen below in Table 2-1. Another major difference is our use of headspace gas chromatography which removed the need to perform any trap to trap distillations.

Table 2-1 below shows the experimental setup of both photolysis, old and new. Past experiments did not deal with constant pressure which affected the error as well as possible methanol production which will be talked about further on.

Table 2-1: Experimental parameters of Boston $[Ru(phen)_3]^{2+}$ system and current photocatalysis system.[4]

	Boston Experimental Parameters	Our Experimental Parameters
Complex	200 µM	225 µM
Ascorbic Acid	0.2 M	0.2 M
Potassium Chloride	0.1 M	0.1 M
Pyridine	0.05 M	0.05 M
Acetonitrile	Not Present in Reactor	49 µM
Reactor Pressure	1~1.5 atm	2.36 atm
Analysis	Trap-Trap Distillation GCMS - Liquid Injection	GCMS - Headspace

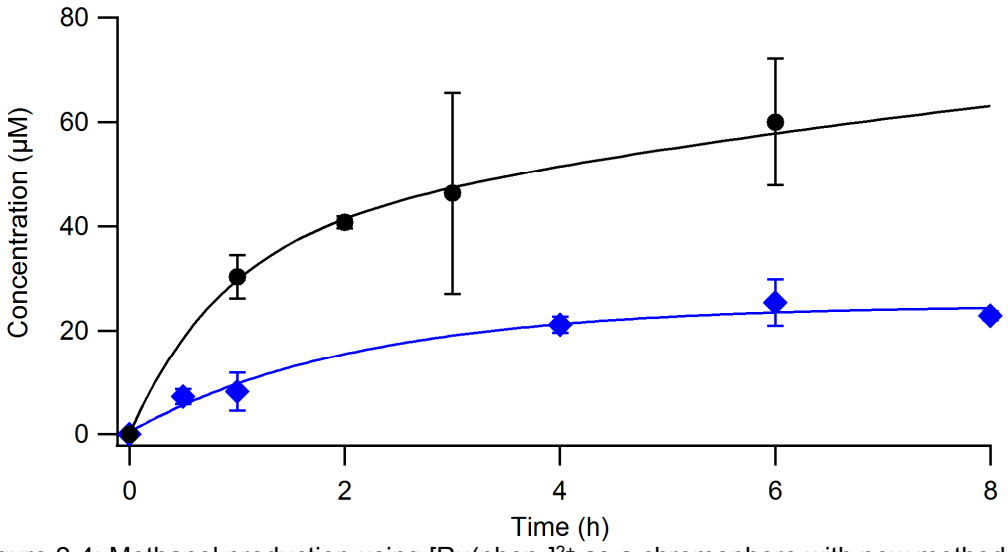

Figure 2-4: Methanol production using $[Ru(phen_3]^{2+}$ as a chromophore with new method (blue), and old method by Boston[4] (black), 0.225 mM $[Ru(phen)_3]Cl_2$, 0.1 M KCl, 0.2 M ascorbic acid, CO_2, at pH 5.0, 25.0 C, 2.36 atm, irradiated at 470 nm.

The new system setup produced three times less methanol than was previously reported, about 20 µM. Methanol production slows and potentially stops after roughly four hours with a max turnover number TON of 0.12 methanol to ruthenium which is roughly three times less than was

previously reported.[4] It was also discovered that varying the pressure yielded no change in methanol concentration.

A source for the differing data could be the change in methanol detection. Previously, methanol was being detected by GC-MS using liquid injection.[4, 36] Liquid injection injects an aliquot of the total sample including the solvent. Our method takes advantage of headspace which has proven to be a much cleaner method. Headspace analysis heats the samples to volatilize the headspace in the sample vial. The headspace is then injected into the gas chromatograph. This method excludes nonvolatile solvents such as water, unless sufficient heat is applied, providing a clean chromatograph. Samples did not have to be treated beforehand with trap to trap distillations as was previously done to remove volatiles, which reduced the associated error and time consumed with sample preparation. Another reason for the low methanol production of our system could be from how the solution is supplied with carbon dioxide after the initial bubbling.[4, 36] Formate is much more prevelant in the solution and thus easier to obtain to reduce, whereas carbon dioxide after bubbling can only be gained by diffusing into the solution from a gas in the headspace due to a constant carbon dioxide headspace pressure of 2.36 atm. A further study could be done to prove this by using an enzyme that increases carbon dioxide diffusion or bubbling carbon dioxide into the solution while the reaction proceeds. The first option would be more ideal in order to keep a constant pressure.

2.3.1.2 System using $[Ru(bpy)_3]^{2+}$

The cage escape yield of $[Ru(phen)_3]^{2+}$ and certain reductive quenchers is unusually low, below 10%.[37, 38] $[Ru(bpy)_3]^{2+}$, on the other hand, has a cage escape yield of 50% with ascorbate, therefore we examined this latter chromophore to see if it improved overall photocatalytic performance.[35] Shown below in Figure 2-5 is the methanol production using $[Ru(bpy)_3]^{2+}$ as a chromophore.

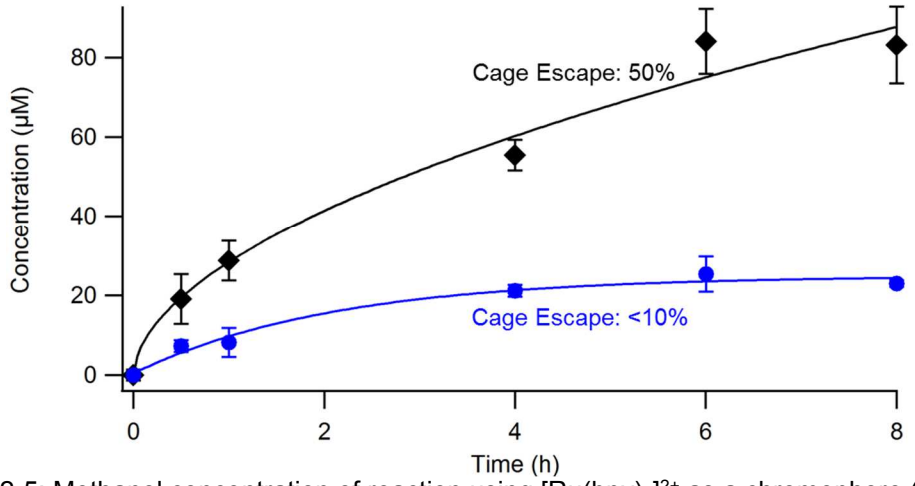

Figure 2-5: Methanol concentration of reaction using $[Ru(bpy)_3]^{2+}$ as a chromophore (black), and the control (blue) over time, 0.225 mM $[Ru(bpy)_3]Cl_2$, 0.2 M ascorbic acid, 0.1 M KCl, CO_2, at pH 5.0, 25.0 C, 2.36 atm, irradiated at 470 nm.

The production of methanol is greater than that of the $[Ru(phen)_3]^{2+}$ system by approximately 20 μM when using $[Ru(bpy)_3]^{2+}$. Methanol is produced for roughly 6-8 hours with little increase after 8 hours. For the 2,2-bipyridine system approximately 0.4 methanol TON were found which is greater than the 0.3 methanol TON of the previous $[Ru(phen)_3]^{2+}$ system by Boston but a four-fold increase versus our own testing with the new analytical method. The trend is the same as the previous data by MacDonnell and Boston in Table 2-2 below.[4] A sample chromatogram is shown below in Figure 2-6. Both the Figure below and Figure 2-8 are of the same 8h time point but different samples.

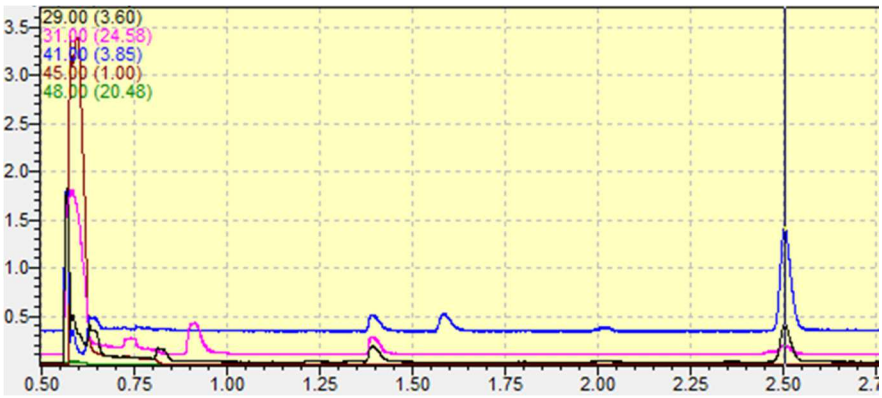

Figure 2-6: Gas Chromatography resulting chromatogram of $[Ru(bpy)_3]^{2+}$ system at 8 h interval showing methanol (0.9 min), and acetonitrile (1.6 min). Method is stated in experimental section above.

Ion chromatography was used to accurately measure the amount of formate produced by the $[Ru(bpy)_3]^{2+}$ system as formate was not detectable by gas chromatograph with the method that was used. The results are shown below in Figure 2-7 with a sample chromatogram being Figure 2-8.

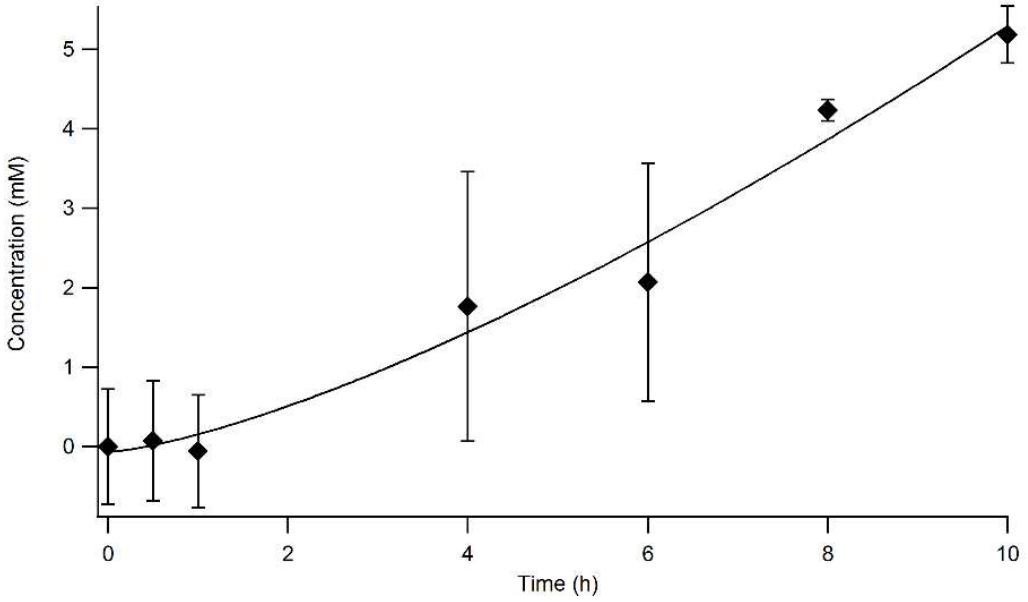

Figure 2-7: Formate concentration via ion chromatography of reaction using $[Ru(bpy)_3]^{2+}$ as a chromophore over time, 0.225 mM $[Ru(bpy)_3]Cl_2$, 0.2 M ascorbic acid, 0.1 M KCl, CO_2, at pH 5.0, 25.0 C, 2.36 atm, irradiated at 470 nm, and filtered through Dionex On Guard II Ag/H Filters

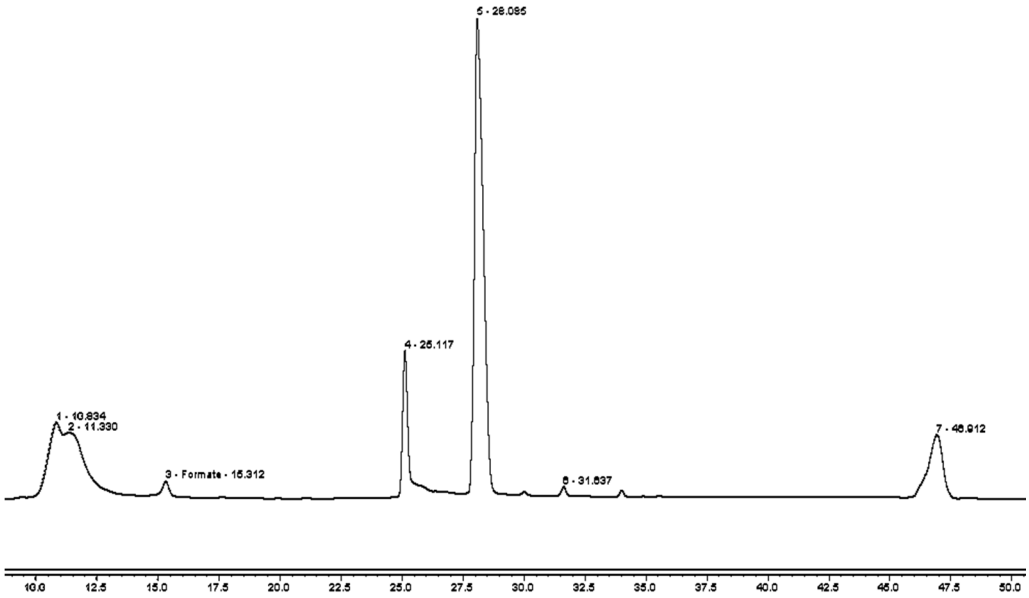

Figure 2-8: Ion chromatography resultant chromatogram of $[Ru(bpy)_3]^{2+}$ sample at 8 h interval where formate appears as the third peak. Method stated above in experimental section.

Figure 2-7 shows the formate production of a photocatalytic system containing complex $[Ru(bpy)_3]^{2+}$ as a chromophore. Formate increases at a slightly increasing rate over the time of the reaction. Formate concentration was determined by ion chromatography but the method was still under development at the time of these experiments. Each sample was filtered once through the On Guard II Ag/H Dionex filters where each sample has its own filter. The samples were kept at 20°C during the analysis and stored in a freezer overnight. The system produced a maximum formate concentration in a ten hour period of 5 mM. This is significantly less than the formate produced in previous literature but as we are producing more methanol it stands to reason that carbon dioxide is being heavily reduced leaving less formate in solution.[4] As the rate of formate increases, methanol production decreases.

Still using the $[Ru(bpy)_3]^{2+}$ as the chromophore we ran experiments to determine if methanol was being produced by the reduction of carbon dioxide or if the system could take the formate that is present, or that it produces, and reduce it to create methanol and other products. For this experiment the solution was degassed with argon and no carbon dioxide was added, instead formic acid was added at the same concentration as the electron donor, ascorbate (0.2 M). The results are shown in Figure 2-9.

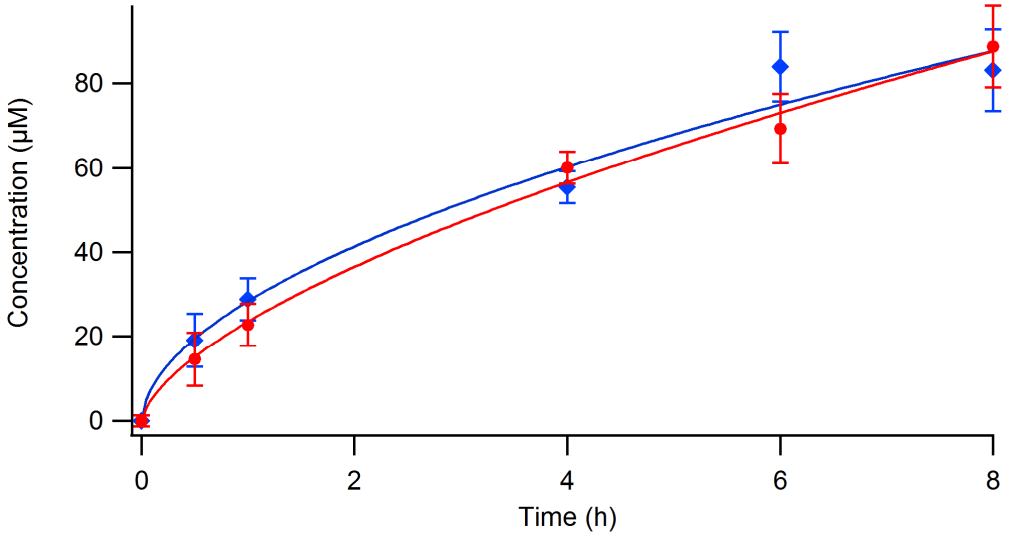

Figure 2-9: Methanol comparison of $[Ru(bpy)_3]^{2+}$ with CO_2 (blue), and without CO_2 with 0.2 M formic acid (red), 0.225 mM $[Ru(bpy)_3]Cl_2$, 0.1 M KCl, 0.2 M ascorbic acid, at pH 5.0, 25.0 C, 2.36 atm, irradiated at 470 nm.

To judge whether formate can enter the reduction cycle formic acid was added to the solution where it was degassed and pressurized with argon instead of carbon dioxide. Both carbon dioxide and formate can be used as a fuel source for the reaction to produce methanol. After the solution is degassed with carbon dioxide, CO_2 can only enter it by diffusing into the solution while the formate is already in the solution. This could account for our lower production of methanol when compared to previous work done by MacDonnell where with not having a constant pressure the system was able to use both carbon dioxide and formate as fuel sources.

Table 2-2: Product analysis of photocatalytic experiments, (a) methanol production after 6 hours, (b) formate production after 1 hour.[4]

		MeOH		Formate	
		Conc. (μM)[a]	TON (in e^-)[a]	Conc. (mM)[b]	TON (in e^-)[b]
$[Ru(phen)_3]^{2+}$	Boston(CO_2)	66±12	0.33 (2.0)	18	76 (152)
	Current(CO_2)	25±2	0.12 (0.76)		
$[Ru(bpy)_3]^{2+}$	CO_2	83±6	0.4 (2.2)	0.06	0.25 (0.51)
	Formic Acid	70±6	0.35 (2.1)		
$[Ru(bqp)_2]^{2+}$	CO_2	40	0.73 (4.4)		

Table 2-2 shows the product results of the all systems that were tested. The new $[Ru(bpy)_3]^{2+}$ system produces more methanol than either controls, Boston and new, while formate is not produced in large quantities until roughly 4 hours, refer to previous figures. Formate production increases as the reaction proceeds while methanol production decreases. Methanol production with $[Ru(bpy)_3]^{2+}$ is greater than the control but does not last much longer, 6-8h. Formate was not the main product as was thought in previous publications. These results could mean that carbon dioxide is reduced to methanol with more effectiveness due to $[Ru(bpy)_3]^{2+}$'s electron transfer efficiency and cage escape even though it's MLCT has slightly less *d*-character from the previous chapter. $[Ru(bqp)_2]^{2+}$ when used as a chromophore produced more methanol than the control but for a much shorter period of time. What is significant that is seen further on is that the methanol produced was done using a drastically reduced concentration of the chromophore.

2.3.1.3 System using $[Ru(bqp)_2]^{2+}$

Studies that have been done previously by Hammarström indicate that $[Ru(bqp)_2]^{2+}$ can possibly reductively quench even faster than the 2,2-bypiridine complex while also being able to transfer electrons at a faster rate (k_{et} < 1 ns) and maintain its emission intensity up to twelve

hours.[12] With this information we suspect that using $[Ru(bqp)_2]^{2+}$ as a chromophore will increase the amount of methanol produced, while increasing the duration of the photocatalytic reaction.

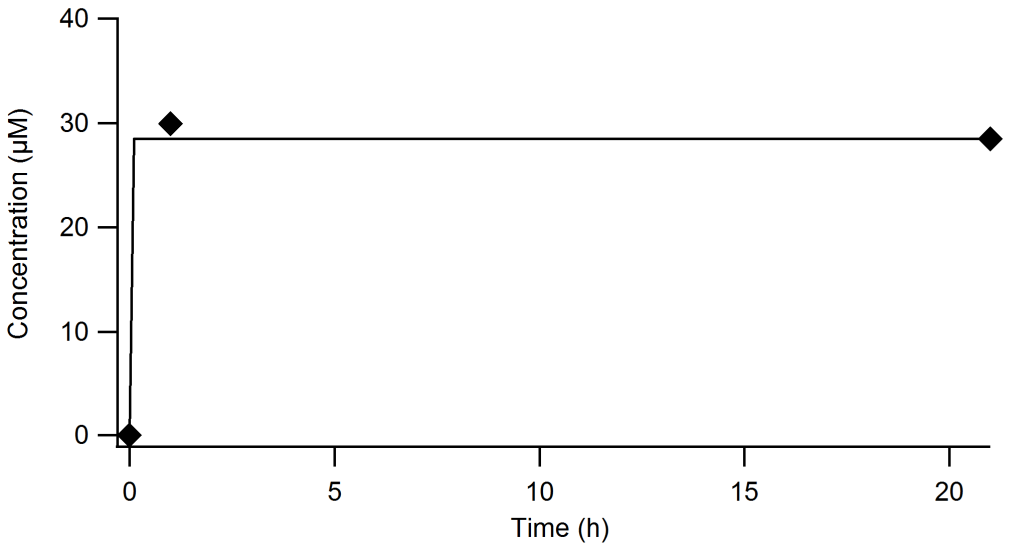

Figure 2-10: Methanol production using $[Ru(bqp)_2]^{2+}$ as a chromophore, 39 μM $[Ru(bqp)_2]Cl_2$, 0.2 M ascorbic acid, 0.1 M KCl, CO_2, at pH 5.0, 25.0 C, 2.36 atm, irradiated at 470 nm.

Shown above in Figure 2-10 were the results when using $[Ru(bqp)_2]^{2+}$ as a chromophore. This is predicted to have the highest methanol production. The figure shows little to no methanol production after one hour of irradiation although due to solubility issues a significantly less amount of complex was used (38.87 μM). Despite the small concentration the reaction still produced a TON of 0.7 MeOH in the first hour. This data is inconclusive in $[Ru(bqp)_2]^{2+}$'s ability to act as a stable, long lasting chromophore but promising in the amount of methanol that could possibly be produced. Due to low synthesis yields further experiments were not able to be conducted.

2.4 Conclusion

When comparing our results to that of previous literature it is found that both $[Ru(bpy)_3]^{2+}$ and $[Ru(bqp)_2]^{2+}$ produce more methanol than the previously used $[Ru(phen)_3]^{2+}$ chromophore.[4]

$[Ru(bpy)_3]^{2+}$ produced greater methanol and had higher TONs than the control while lasting slightly longer, up to 6-8 hours, making it to be the better choice when compared to $[Ru(phen)_3]^{2+}$. This is attributed to possible faster reductive quenching, depending on the sacrificial donor, and electron transfer rates reported by Castellano along with its longer emission lifetime resulting from less *d*-character of its MLCT states causing a separation of the ^{3}MLCT and ^{3}MC states in comparison to $[Ru(phen)_3]^{2+}$.[35, 34, 41] The system using $[Ru(bpy)_3]^{2+}$ as the chromophore produced less formate than previously reported for the control but also had a comparable increase in methanol production. From this can assume that the carbon dioxide is being reduced straight to methanol. This is a prime example of $[Ru(bpy)_3]^{2+}$'s electron efficiency and cage escape reported by Castellano.[35] Carbon dioxide does not need to be present for methanol to be produced. While is it shown that carbon dioxide is the slightly more favored reactant, but over time as shown in Figure 2-6 that may change.

While the data on $[Ru(bqp)_2]^{2+}$ is inconclusive it does warrant further study as the TON indicates its high electron efficiency and potential as a chromophore. It also has even less mixing of its E_g *d* orbitals with its MLCT states than $[Ru(bpy)_3]^{2+}$ causing an even further separation between the MLCT and MC states allowing for stability of the ^{3}MLCT state and a much longer lifetime emission shown in chapter 1.

References

1. Seshadri, G.; Lin, C.; Bocarsly, A. B., A new homogeneous electrocatalyst for the reduction of carbon dioxide to methanol at low overpotential. *J. Electroanal. Chem.* **1994,** *372* (1–2), 145-150.

2. Willner, I.; Maidan, R.; Mandler, D.; Duerr, H.; Doerr, G.; Zengerle, K., Photosensitized reduction of carbon dioxide to methane and hydrogen evolution in the presence of ruthenium and osmium colloids: strategies to design selectivity of products distribution. *J. Am. Chem. Soc.* **1987,** *109* (20), 6080-6086.

3. Bolinger, C. M.; Story, N.; Sullivan, B. P.; Meyer, T. J., Electrocatalytic reduction of carbon dioxide by 2,2'-bipyridine complexes of rhodium and iridium. *Inorg. Chem.* **1988,** *27* (25), 4582-4587.

4. Boston, D. J.; Xu, C.; Armstrong, D. W.; MacDonnell, F. M., Photochemical Reduction of Carbon Dioxide to Methanol and Formate in a Homogeneous System with Pyridinium Catalysts. *J. Am. Chem. Soc.* **2013,** *135* (44), 16252-16255.

5. Boston, D.; Huang, K.-L.; de Tacconi, N.; Myung, N.; MacDonell, F.; Rajeshwar, K., CHAPTER 11 Electro- and Photocatalytic Reduction of CO2: The Homogeneous and Heterogeneous Worlds Collide? In *Photoelectrochemical Water Splitting: Materials, Processes and Architectures*, The Royal Society of Chemistry: 2013; pp 289-332.

6. Borg, O. A.; Godinho, S. S. M. C.; Lundqvist, M. J.; Lunell, S.; Persson, P., Computational Study of the Lowest Triplet State of Ruthenium Polypyridyl Complexes Used in Artificial Photosynthesis. *J. Phys. Chem. A.* **2008,** *112* (19), 4470-4476.

7. Zheng, K. C.; Wang, J. P.; Liu, X. W.; Shen, Y.; Yun, F. C., Studies of substituent effects on the electronic structure and related properties of [Ru(phen)3]2+ with DFT method. *J. Mol. Struct.* **2002,** *577* (2–3), 95-105.

8. Durham, B.; Caspar, J. V.; Nagle, J. K.; Meyer, T. J., Photochemistry of tris(2,2'-bipyridine)ruthenium(2+) ion. *J. Am. Chem. Soc.* **1982,** *104* (18), 4803-4810.

9. Caspar, J. V.; Meyer, T. J., Photochemistry of tris(2,2'-bipyridine)ruthenium(2+) ion (Ru(bpy)32+). Solvent effects. *J. Am. Chem. Soc.* **1983,** *105* (17), 5583-5590.

10. Österman, T.; Abrahamsson, M.; Becker, H.-C.; Hammarström, L.; Persson, P., Influence of Triplet State Multidimensionality on Excited State Lifetimes of Bis-tridentate RuII Complexes: A Computational Study. *J. Phys. Chem. A.* **2012,** *116* (3), 1041-1050.

11. Hewitt, J. T.; Vallett, P. J.; Damrauer, N. H., Dynamics of the 3MLCT in Ru(II) Terpyridyl Complexes Probed by Ultrafast Spectroscopy: Evidence of Excited-State Equilibration and Interligand Electron Transfer. *J. Phys. Chem. A.* **2012,** *116* (47), 11536-11547.

12. Abrahamsson, M.; Jäger, M.; Kumar, R. J.; Österman, T.; Persson, P.; Becker, H.-C.; Johansson, O.; Hammarström, L., Bistridentate Ruthenium(II)polypyridyl-Type Complexes with Microsecond 3MLCT State Lifetimes: Sensitizers for Rod-Like Molecular Arrays. *J. Am. Chem. Soc.* **2008,** *130* (46), 15533-15542.

13. Lashgari, K.; Kritikos, M.; Norrestam, R.; Norrby, T., Bis(terpyridine)ruthenium(II) bis(hexafluorophosphate) diacetonitrile solvate. *Acta Cryst.* **1999,** *55* (1), 64-67.

14. Abrahamsson, M.; Jäger, M.; Österman, T.; Eriksson, L.; Persson, P.; Becker, H.-C.; Johansson, O.; Hammarström, L., A 3.0 μs Room Temperature Excited State Lifetime of a Bistridentate RuII−Polypyridine Complex for Rod-like Molecular Arrays. *J. Am. Chem. Soc.* **2006,** *128* (39), 12616-12617.

15. Medlycott, E. A.; Hanan, G. S., Designing tridentate ligands for ruthenium(ii) complexes with prolonged room temperature luminescence lifetimes. *Chem. Soc. Rev.* **2005,** *34* (2), 133-142.

16. Král, M., The ligand-ligand and spin-orbit interactions in Fe(phen) 3 +2 and Ru(phen) 3 +2 ions. *Theoret. Chim. Acta* **1980,** *55* (4), 333-336.

17. Zheng, K. C.; Wang, J. P.; Peng, W. L.; Liu, X. W.; Yun, F. C., Theoretical studies on the electronic structures and related properties of [Ru(L)3]2+ (L=bpy, bpm, bpz) with DFT method. *J. Mol. Struct.* **2002,** *582* (1–3), 1-9.

18. Li, J.; Chen, J.-C.; Xu, L.-C.; Zheng, K.-C.; Ji, L.-N., A DFT/TDDFT study on the structures, trend in DNA-binding and spectral properties of molecular “light switch” complexes [Ru(phen)2(L)]2+(L = dppz, taptp, phehat). *J. Organomet. Chem.* **2007,** *692* (4), 831-838.

19. Jakubikova, E.; Chen, W.; Dattelbaum, D. M.; Rein, F. N.; Rocha, R. C.; Martin, R. L.; Batista, E. R., Electronic Structure and Spectroscopy of [Ru(tpy)2]2+, [Ru(tpy)(bpy)(H2O)]2+, and [Ru(tpy)(bpy)(Cl)]+. *Inorg. Chem.* **2009,** *48* (22), 10720-10725.

20. Maloney, D. J.; MacDonnell, F. M., [Lambda]-Tris(1,10-phenanthroline-N,N')ruthenium(II) Bis(hexafluorophosphate)-Acetonitrile-Diethyl Ether (1/1/0.5). *Acta Cryst.* **1997,** *53* (6), 705-707.

21. Rillema, D. P.; Jones, D. S., Structure of tris(2,2[prime or minute]-bipyridyl)ruthenium(II) hexafluorophosphate, [Ru(bipy)3][PF6]2; X-ray crystallographic determination. *J.C.S. Chem. Comm.* **1979,** (19), 849-851.

22. Jäger, M.; Kumar, R. J.; Görls, H.; Bergquist, J.; Johansson, O., Facile Synthesis of Bistridentate RuII Complexes Based on 2,6-Di(quinolin-8-yl)pyridyl Ligands: Sensitizers with Microsecond 3MLCT Excited State Lifetimes. *Inorg. Chem.* **2009,** *48* (7), 3228-3238.

23. ZHOU, X.; REN; #160; Ai-Min; FENG; #160; Ji-Kang, Theoretical studies on the ground states in M(terpyridine)[2][+][2] and M(n-butyl-phenylterpyridine)[2][+][2] (M = Fe, Ru, Os) and excited states in Ru(terpyridine)[2][+][2] using density functional theory. 2005, pp 338-347.

24. Ackermann, M. N.; Interrante, L. V., Ruthenium(II) complexes of modified 1,10-phenanthrolines. 1. Synthesis and properties of complexes containing dipyridophenazines and a dicyanomethylene-substituted 1,10-phenanthroline. *Inorg. Chem.* **1984,** *23* (24), 3904-3911.

25. de Carvalho, I. M. M.; de Sousa Moreira, Í.; Gehlen, M. H., Luminescence study of Ru(II) bipyridine–acridine spaced by amide and proline bridges. *Polyhedron* **2005,** *24* (1), 65-73.

26. Mandler, D.; Willner, I., Effective photoreduction of carbon dioxide/bicarbonate to formate using visible light. *J. Am. Chem. Soc.* **1987,** *109* (25), 7884-7885.

27. Barton Cole, E.; Lakkaraju, P. S.; Rampulla, D. M.; Morris, A. J.; Abelev, E.; Bocarsly, A. B., Using a One-Electron Shuttle for the Multielectron Reduction of CO2 to Methanol: Kinetic, Mechanistic, and Structural Insights. *J. Am. Chem. Soc.* **2010,** *132* (33), 11539-11551.

28. Keith, J. A.; Carter, E. A., Theoretical Insights into Pyridinium-Based Photoelectrocatalytic Reduction of CO2. *J. Am. Chem. Soc.* **2012,** *134* (18), 7580-7583.

29. Lim, C.-H.; Holder, A. M.; Musgrave, C. B., Mechanism of Homogeneous Reduction of CO2 by Pyridine: Proton Relay in Aqueous Solvent and Aromatic Stabilization. *J. A. Chem.Soc.* **2013,** *135* (1), 142-154.

30. Tossell, J. A., Calculation of the properties of molecules in the pyridine catalyst system for the photochemical conversion of CO2 to methanol. *Comp. Theor. Chem.* **2011,** *977* (1–3), 123-127.

31. Barton, E. E.; Rampulla, D. M.; Bocarsly, A. B., Selective Solar-Driven Reduction of CO2 to Methanol Using a Catalyzed p-GaP Based Photoelectrochemical Cell. *J. Am. Chem. Soc.* **2008,** *130* (20), 6342-6344.

32. Yan, Y.; Zeitler, E. L.; Gu, J.; Hu, Y.; Bocarsly, A. B., Electrochemistry of Aqueous Pyridinium: Exploration of a Key Aspect of Electrocatalytic Reduction of CO2 to Methanol. *J. Am. Chem. Soc.* **2013,** *135* (38), 14020-14023.

33. Li, C.; Hoffman, M. Z., Electron Localization or Delocalization in the MLCT Excited States of Ru(bpy)32+ and Ru(phen)32+. Consequences to Their Photochemistry and Photophysics in Fluid Solution. *Inorg. Chem.* **1998,** *37* (4), 830-832.

34. Krishnan, C. V.; Creutz, C.; Mahajan, D.; Schwarz, H. A.; Sutin, N., Homogeneous Catalysis of the Photoreduction of Water by Visible Light. 3. Mediation by Polypyridine Complexes of Ruthenium(II) and Cobalt(II). *Isr. J. Chem.* **1982,** *22* (2), 98-106.

35. Khnayzer, R. S.; Thoi, V. S.; Nippe, M.; King, A. E.; Jurss, J. W.; El Roz, K. A.; Long, J. R.; Chang, C. J.; Castellano, F. N., Towards a comprehensive understanding of visible-light photogeneration of hydrogen from water using cobalt(ii) polypyridyl catalysts. *Energy Environ. SCi.* **2014,** *7* (4), 1477-1488.

36. Boston, D. J.; Pachón, Y. M. F.; Lezna, R. O.; de Tacconi, N. R.; MacDonnell, F. M., Electrocatalytic and Photocatalytic Conversion of CO2 to Methanol using Ruthenium Complexes with Internal Pyridyl Cocatalysts. *Inorg. Chem.* **2014,** *53* (13), 6544-6553.

37. Lin, C. T.; Boettcher, W.; Chou, M.; Creutz, C.; Sutin, N., Mechanism of the quenching of the emission of substituted polypyridineruthenium(II) complexes by iron(III), chromium(III), and europium(III) ions. *J. Am. Chem. Soc.* **1976,** *98* (21), 6536-6544.

38. Olmsted, J.; Meyer, T. J., Factors affecting cage escape yields following electron-transfer quenching. *J. Phys. Chem.* **1987,** *91* (6), 1649-1655.

39. Matsumura-Inoue, T.; Tanabe, M.; Minami, T.; Ohashi, T., A Remarkably Rapid Synthesis of Ruthenium(II) Polypyridine Complexes by Microwave Irradiation. *Chem. Lett.* **1994,** *23* (12), 2443-2446.

40. Dass, C., Quantitative Analysis. In *Fundamentals of Contemporary Mass Spectrometry*, John Wiley & Sons, Inc.: 2006; pp 485-499.

41. Krishnan, C. V.; Sutin, N., Homogeneous catalysis of the photoreduction of water by visible light. 2. Mediation by a tris(2,2'-bipyridine)ruthenium(II)-cobalt(II) bipyridine system. *J. Am. Chem. Soc.* **1981,** *103* (8), 2141-2142.

Biographical Information

Matthew West has spent his entire collegiate academic career at The University of Texas at Arlington since beginning in 2008. During this time he has exclusively worked under Dr. Frederick MacDonnell on photocatalytic reduction of carbon dioxide as well as some electrocatalytic reduction of carbon dioxide.